

<sub>1</sub> Determining multi-scale controls on river  
<sub>2</sub> temperature: a time series approach

<sub>3</sub> Michael Vlah

<sub>4</sub> March 31, 2017

## 5 Abstract

6 Temperature is among the most important determinants of riverine biodiversity  
7 and health. It is therefore a primary freshwater management concern, particu-  
8 larly where cold-water fish are of high ecological, recreational, and commercial  
9 value. However, river temperature in the Puget Sound watershed of the North-  
10 western U.S.A. is affected by a great diversity of drivers at multiple spatial and  
11 temporal scales, and little is known of their interactions. We used dynamic  
12 factor analysis, a multivariate time-series technique, to examine relationships  
13 among these drivers, synthesizing long-term climate and fine-scale landcover  
14 data. We found that primarily rain-fed rivers experience large seasonal temper-  
15 ature fluctuations, which closely track atmospheric temperature, while snow-fed  
16 rivers tend to be weakly, and in some cases inversely, coupled with such fluc-  
17 tuations. Among watersheds, groundwater influx, land slope, and Q further  
18 augment or dampen these relationships. Our results suggest the temperature  
19 of high-elevation rivers, absent the influence of ice, should be highly variable,  
20 and that glacially fed streams stand to see the largest changes in temperature  
21 regime under proposed climate scenarios.

## 22 Introduction

23 The ecological condition of a stream or river, the life it supports, and the goods  
24 and services it provides, are influenced by the timing and magnitude of sea-  
25 sonal changes in water temperature. Temperature is a chief consideration in  
26 the management of fisheries, as it affects species distribution (?), growth and  
27 reproduction (?), and migration timing (?). In particular, In the Puget Sound  
28 watershed of the American Pacific Northwest, several salmonid species spawn,  
29 migrate, and emerge only within the bounds of a few degrees Celsius, and thrive  
30 under even greater temperature constraints (?). As a result, the success of com-  
31 mercial and recreational fisheries that depend on the region’s riverine habitat  
32 rests on many precarious factors.

33 River networks, being fractal in structure, are naturally governed by envi-  
34 ronmental processes at multiple scales. Seasonal variation in water temperature  
35 in rivers of the Pacific Northwest is a function of the surrounding air, as well  
36 as precipitation and snowmelt (?). These drivers may in turn be mediated or  
37 supplemented by several aspects of watershed morphology at smaller scales, in-  
38 cluding slope, elevation, and geology (??). Taken together, this hierarchical  
39 system complicates fishery management, as the temperature regime of one river  
40 may be the direct product of climate, while that of another may depend more  
41 on within-watershed conditions.

42 Adding to this picture, flow regimes across rivers of the Puget Sound wa-  
43 tershed vary with latitude and elevation (??), and can be classified broadly  
44 into three categories by flow source and hydrograph shape. Rain-dominated  
45 (RD) rivers receive little or no input from snowmelt, and thus peak in discharge  
46 (Q) during the rainy season, usually between October and February. Snow-  
47 dominated (SD) rivers instead see peak flow during spring snowmelt, often in  
48 April, May, or June. Between these extremes lies a third class of rain-and-snow-  
49 driven (RS) rivers, which have appreciable peaks at both times.

50 Effective management plans must therefore integrate a diversity of factors  
51 across space and time in order to determine which rivers and watersheds are  
52 likely to see consequential changes under projected climate and land use scenar-  
53 ios for the Pacific Northwest (??). However, the understanding required to do  
54 so is limited by knowledge of relationships among temperature drivers at scale.

55 We sought to identify streams in the Puget Sound region whose temperatures  
56 fluctuate closely with regional trends in air temperature, precipitation, and  
57 snowmelt, and those that depart from regional patterns. Our second aim was  
58 to identify watershed features that correlate with such departures, and thus  
59 provide a nuanced basis for predicting impacts of water temperature on aquatic  
60 biodiversity and fishery health. We hypothesized that water temperature ( $T_{\text{water}}$ )  
61 would track air temperature  $T_{\text{air}}$  most closely in RD rivers (??). We expected  
62 deviations from this relationship to correlate best with cold-water influx from  
63 snow and ice melt (?) and with factors affecting heat capacity of water, including  
64 Q (volume over time) and watershed slope (which relates to turbulence, surface  
65 area, and mixing; ?).

## 66 **Methods**

### 67 **Water and climate data**

68 We investigated climate and landscape controls on  $T_{\text{water}}$  and  $Q$ , as separate re-  
69 sponse variables, from 1978 to 2015. Monthly time series of water temperature  
70 were obtained for 24 river sites via the Washington Department of Ecology’s  
71 River and Stream Water Quality Monitoring program (?). These sites repre-  
72 sent 19 nonnested watersheds across 9 counties, and range from 4 to 775 m in  
73 elevation. For at least one site at each river, monthly  $Q$  time series were also  
74 available, either from the same location as one of the temperature monitoring  
75 sites, or from within 30 km on the same major reach.  $Q$  data were aggregated  
76 by monthly mean from the USGS National Water Information System database  
77 (?).

78

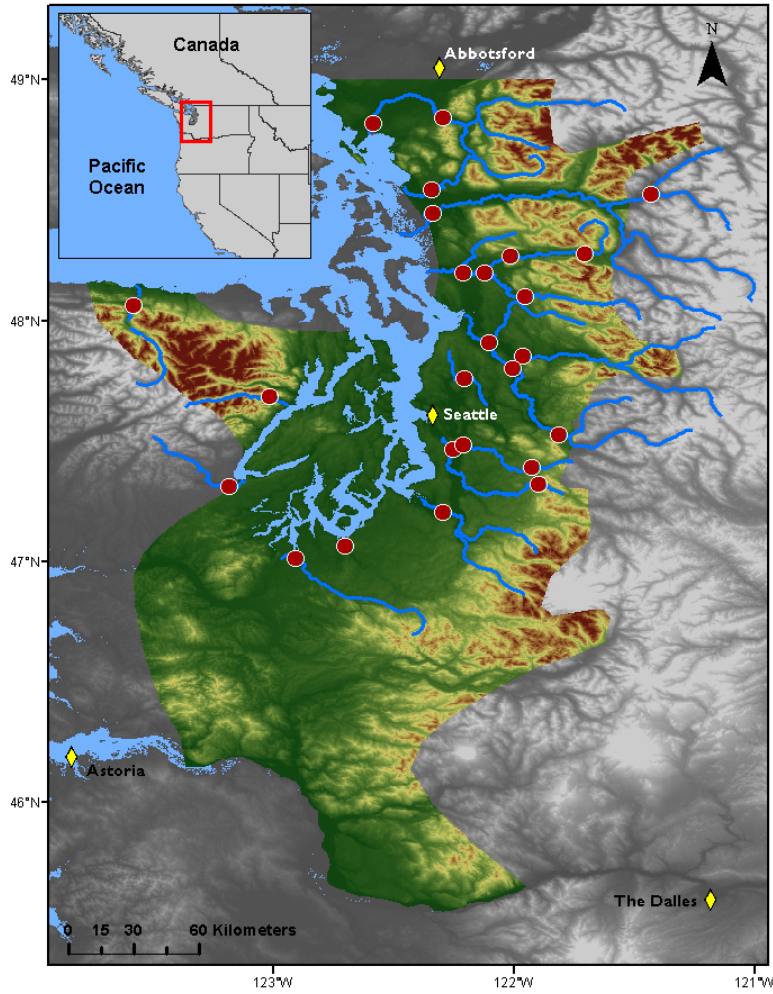


**Figure 1** Site locations (red points) in relation to combined Washington State Climate Divisions 3 and 4 (colored topography), the region across which climate data were aggregated.

Potential climatic predictors of  $T_{\text{water}}$  and  $Q$  included mean and max  $T_{\text{air}}$  ( $^{\circ}\text{C}$ ), total precipitation (cm), snowmelt (cm), and hydrological drought (Palmer Hydrological Drought Index), averaged by month across the response variable time series. All but snowmelt were available through the U.S. Climate Divisional Dataset, developed by the National Centers for Environmental Informa-

tion (NCEI; ?). We acquired climatic predictor data grouped by Washington State climate division, and all but two of our sites fell within divisions 3 (Puget Sound Lowland) and 4 (East Olympic/Cascade Foothills; see Fig. 1). We therefore aggregated these data by monthly mean across the two regions (after verifying their post-standardization similarity), resulting in a single dataset of four climatic predictor variables. A snowmelt time series was then added to this dataset, using monthly mean records from six SNOTEL sites (Bumping Ridge, Elbow Lake, Mount Crag, Park Creek Ridge, Stevens Pass, White Pass) listed by the USDA’s Natural Resources Conservation Service; ?. We calculated monthly snowmelt for each site as the absolute value of negative differences in cumulative snow water equivalent from each month to the next. The snowmelt time series was assigned zeros for any positive differences (accumulations).

## Time series analysis

Response time series ( $T_{\text{water}}$  and  $Q$ ) were modeled using dynamic factor analysis (DFA; ?), a multivariate technique that can be thought of as an analog to principal component analysis in the time domain. In DFA, response time series are fit with a linear combination of shared, random-walk trends (usually many fewer than the total number of response series), predictors (which can have unique effects on each response series), and random error. We chose DFA over a traditional multivariate state space approach for two reasons. First, it provides advantages in computational efficiency, as a small number of shared trends often adequately capture variation across dozens of responses, and at much lower parameter cost (?). Second, in terms of identifying what drives the shared trends, having fewer of them allows for greater inferential parsimony. Being a multivariate technique, DFA also provides an advantage over univariate alternatives in that covariance structure among responses can be specified and compared. All models were fit using maximum likelihood estimation by automatic differentiation, with Template Model Builder software (?), which we called using package TMB in R (??).

DFA takes the following form:

$$\mathbf{x}_t = \mathbf{x}_{t-1} + \mathbf{w}_t, \text{ where } \mathbf{w}_t \sim \text{MVN}(0, \mathbf{Q}) \quad (1)$$

$$\mathbf{y}_t = \mathbf{Z}\mathbf{x}_t + \mathbf{D}\mathbf{d}_t + \mathbf{v}_t, \text{ where } \mathbf{v}_t \sim \text{MVN}(0, \mathbf{R}) \quad (2)$$

$$\mathbf{x}_0 \sim \text{MVN}(0, \mathbf{\Lambda}) \quad (3)$$

At time step  $t$ , the  $m \times 1$  vector of shared trends ( $\mathbf{x}$ ) is a function of  $\mathbf{x}$  in the previous step, plus normal error ( $\mathbf{w}$ ;  $m \times 1$ ; Eq. 1). This is the definition of a random walk. The  $n \times 1$  response vector ( $\mathbf{y}$ ) at time  $t$  is a function of the shared trends and their factor loadings ( $\mathbf{Z}$ ;  $n \times m$ ), covariates ( $\mathbf{d}$ ;  $q \times 1$ ) and their river-specific effects ( $\mathbf{D}$ ;  $n \times q$ ), and a second normal error term ( $\mathbf{v}$ ;  $n \times 1$ ; Eq. 2).  $\mathbf{R}$  and  $\mathbf{Q}$  are variance-covariance matrices of order  $m$ , and  $\mathbf{Q}$  is set to identity for model identifiability (?). The initial state of the shared trend vector ( $\mathbf{x}_0$ ) is multivariate-normally distributed with a mean of zero and a diagonal variance-covariance matrix with large variance (e.g. 5; Eq. 3). Response and predictor

data were standardized to facilitate comparison of effect sizes and avoid error inflation.

Because we were interested in isolating the effects of climatic predictors on  $T_{\text{water}}$  and  $Q$ , we used a fixed factor to account for recurring seasonal variation not related to the predictors, with one factor level for each month. This factor was incorporated into the covariate matrix ( $\mathbf{d}$ ). Thus, the coefficient in  $\mathbf{D}$  relating, say, precipitation (predictor) and  $T_{\text{water}}$  (response), represents the effect size of the former on the latter. In other words, it is the change in water temperature accompanying a unit change in precipitation across the whole time series. We call this relationship "coupling." We were also interested in coupling by month for  $T_{\text{air}}$ , which required that it be arranged as twelve separate, monthly time series. Concretely,

$$\mathbf{d} = \begin{matrix} & \text{Jan}_{1978} & \text{Feb}_{1978} & \text{Mar}_{1978} & \cdots & \text{Dec}_{2015} \\ \begin{matrix} 1 \\ 2 \\ 3 \\ \vdots \\ 12 \\ 13 \\ 14 \\ 15 \\ 16 \\ 17 \\ \vdots \\ 26 \end{matrix} & \left( \begin{array}{ccccc} 1 & 0 & 0 & \cdots & 0 \\ 0 & 1 & 0 & \cdots & 0 \\ 0 & 0 & 1 & \cdots & 0 \\ \vdots & \vdots & \vdots & \ddots & \vdots \\ 0 & 0 & 0 & \cdots & 1 \\ \text{precip}_1 & \text{precip}_2 & \text{precip}_3 & \cdots & \text{precip}_T \\ \text{snowmelt}_1 & \text{snowmelt}_2 & \text{snowmelt}_3 & \cdots & \text{snowmelt}_T \\ \text{air}_1 & 0 & 0 & \cdots & 0 \\ 0 & \text{air}_2 & 0 & \cdots & 0 \\ 0 & 0 & \text{air}_3 & \cdots & 0 \\ \vdots & \vdots & \vdots & \ddots & \vdots \\ 0 & 0 & 0 & \cdots & \text{air}_T \end{array} \right) \end{matrix}$$

is the covariate matrix structure necessary to account for seasonal variation of unknown origin (rows 1-12), and the effects of precipitation (row 13) and snowmelt (row 14), while also yielding the effect of  $T_{\text{air}}$  by month (rows 15-26) on the response ( $\mathbf{y}$ ; Eq. 2). This is the covariate structure of the  $T_{\text{water}}$  model we used for subsequent analyses, not including those described in Figure 5d-e, and Appendix B. The same form was used for the  $Q$  model.

Additional, non seasonal variation due to unknown factors manifests in the shared trends, and a portion of any residual variation is absorbed by error matrix  $\mathbf{v}$ . We fit models using four unique error structures ( $\mathbf{R}$ ), to allow for multiple suites of unknown drivers affecting rivers. We included shared variance with zero covariance, individual variance with zero covariance, shared variance with shared covariance, and individual variance with individual covariance. Details on these structures and their implications can be found in (?). The best models for  $T_{\text{water}}$  and  $Q$  were determined via AIC. However, negligible likelihood improvements can be inflated when multiplied by thousands of data points, undermining common rules of thumb for admitting additional parameters under AIC (?). Thus, we had reason to doubt that the "most parsimonious" model

according to AIC alone was any better than a much simpler alternative. To manage this, we required that each additional trend, covariate, or seasonal structure improve the median coefficient of determination ( $R^2$ ) by at least 1% in order to justify accepting its attendant complexity.

## Landscape predictors and post-hoc regression

For post-hoc analyses, monitoring sites were separated into three classes based on relative areal coverage of perennial ice and/snow (hereinafter “% glaciation”) and mean elevation across their watersheds. The three classes are loosely based on the classification scheme and language of the Climate Impacts Group at the University of Washington (?), and are here delineated according to Table 1.

**Table 1** Watershed classification scheme

Classification	Abb.	Glaciation (%)	Mean elev. (m)
Rain-dominated	RD	$< 0.7$	$< 600$
Rain-and-snow	RS	$< 0.7$	$\geq 600$
Snow-dominated	SD	$\geq 0.7$	-

After model selection, climatic predictor effect sizes ( $\mathbf{D}$ ; Eq. 2) for each river were back-transformed to their original scales and regressed against landscape predictors in order to identify possible watershed-scale controls on coupling. To achieve this, we amassed an additional dataset of landscape features. These were collected individually for each of the watersheds corresponding to our 24 river sites, using the EPA’s StreamCat (stream-catchment) data library (?) and the National Hydrography Dataset (NHDPlusV2; ?). Each site was mapped to an individual river reach, defined as a segment bounded on each end by a stream or river source, confluence, or mouth. The region contributing flow to this reach (its watershed) was then fetched, along with selected areal data, from the NHDPlusV2 database. Landscape attributes used as predictors were aggregated by watershed mean where applicable, and include elevation (m), total area ( $\text{km}^2$ ), soil permeability ( $\text{cm hr}^{-1}$ ), water table depth (cm), bedrock depth (cm), Base Flow Index (BFI; %), runoff ( $\text{mm mo}^{-1}$ ), percent perennial ice and snow coverage (National Land Cover Database [NLDC] 2006 and 2011 average), riparian population density (people  $\text{km}^{-2}$  within 100m of streams; 2010 census), riparian road density ( $\text{km km}^{-2}$ ; 2010 census), and percent riparian urban land (NLCD 2011). Monitoring site elevation (m) and presence of upstream dams (as full/partial/no damming of upstream mainstem and major tributaries) were also included. Finally, we calculated area above 1000 m (as % watershed area), mean slope (% rise), and mean aspect (degree from true north) by delineating and summarizing watersheds from a digital elevation model in ArcMap v. 10.4 (?).

An additional set of post-hoc regressions was performed using factor loadings on shared trends ( $\mathbf{Z}$ ; Eq.2) as dependent variables, with landscape predictors again as independent variables. Loadings represent the degree to which each river’s temperature fluctuates with the anonymous force driving the corresponding shared trend. A landscape feature that varies in proportion to these

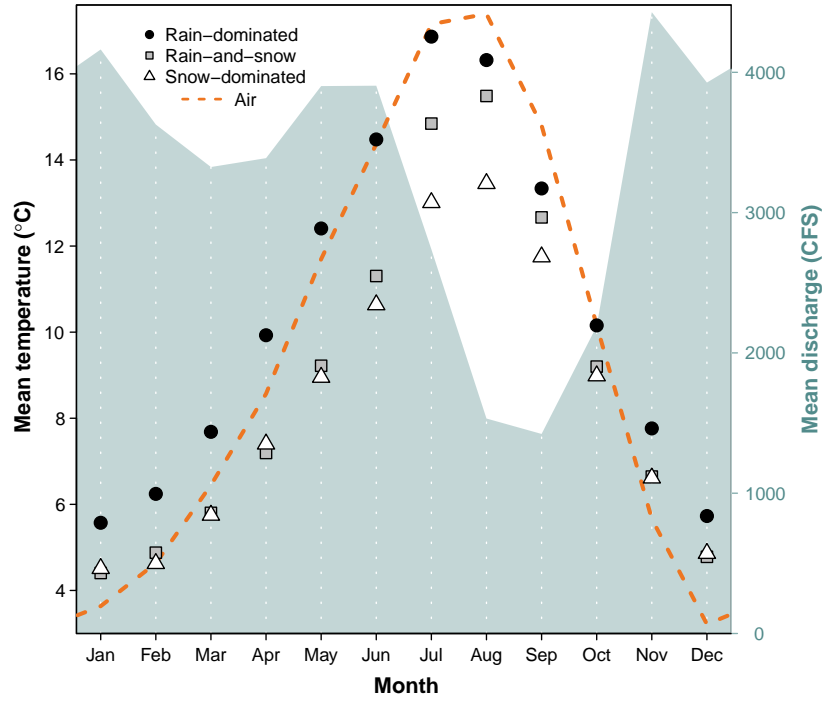


loadings is therefore likely to be a mediator of the anonymous force, if not the force itself. To facilitate inference by way of the shared trends, we made three simplifications to the model. We removed the monthly factor and the snowmelt predictor from the covariate matrix (**d**, rows 1-12 and 14), so that the trends would be free to express seasonal and elevational variation. Then, we limited the number of trends to between one and three, to avoid "trend specialization." in other words, we optimized the trends for flexibility while concentrating their explanatory power. Additionally, we ordinated the landscape predictors with principal coordinates analysis (PCoA), as a way to conceptually "group" them by correlation. Data constrained to irregular, restricted ranges were scaled to [0-1] and arcsine-square-root transformed, along with all proportional data (The logit transform was avoided to prevent generation of infinite values.). All continuous data were then centered and scaled to unit variance before PCoA was performed. We used the Gower dissimilarity coefficient (Gower's distance) to account for association among both continuous and nominal variables (?).

## Results

Mean monthly temperature trends for the three river classes, aggregated across all 38 years of data, deviated by a minimum of 1.0°C in December, and a maximum of 3.9°C in July (Fig. 2). SD rivers remained approximately two degrees colder than their RS counterparts through mid-late summer, and 3-4 degrees colder than RD throughout spring and summer. RD rivers were consistently warmest throughout the year. In January, RS reached a minimum of 4.4°C, and did not significantly differ from SD (Student's t:  $p < 0.01$ ,  $F = 11.9$ ). RD only attained a minimum of 5.6°C. RS reached a peak summer temperature of 16.9°C in July, while RS and SD followed in August with peak temperatures of 15.5 and 13.5°C, respectively.

Meanwhile, the amplitude of  $T_{\text{air}}$  oscillation exceeded that of any river class, dipping below  $T_{\text{water}}$  in autumn to a minimum of 3.2°C in December, and rising above RS and SD in March to an August maximum of 17.4°C.  $T_{\text{air}}$  did not overtake RD  $T_{\text{water}}$  until August, by which time the latter had begun to decline.



229

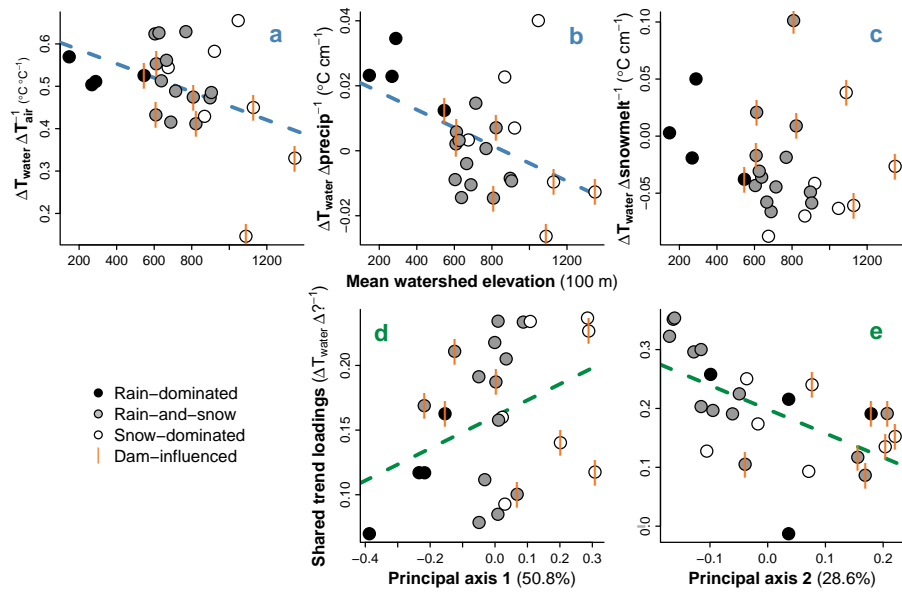
230 **Figure 2** Monthly mean  $T_{\text{water}}$  by river class, and  $T_{\text{air}}$  and  $Q$  across classes,  
 231 from 1978 to 2015. All depicted series represent discrete data.

232

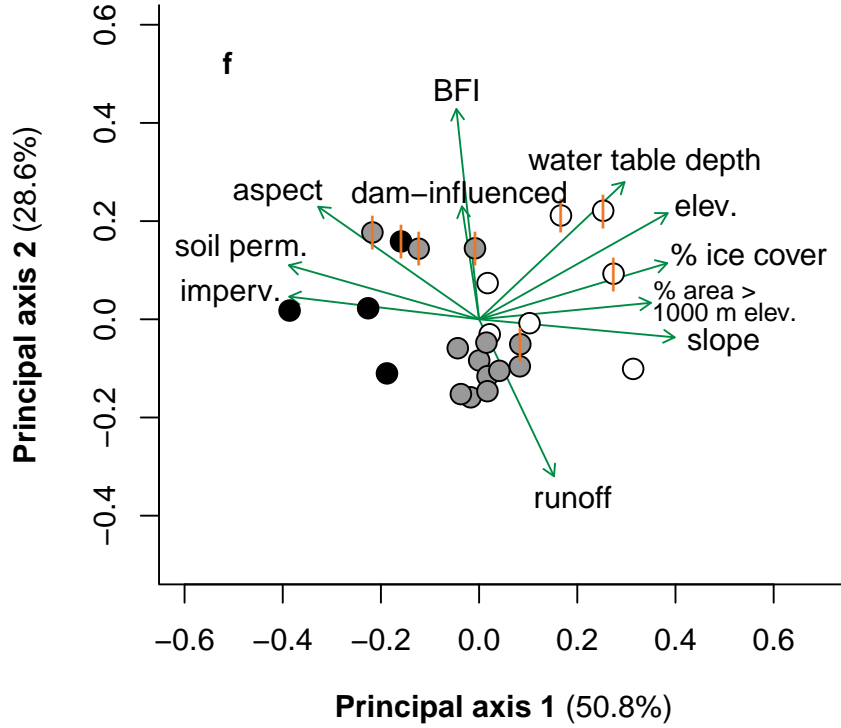
233 The combined hydrograph of all rivers revealed two primary peaks, one be-  
 234 ginning in late spring and the other extending from late fall to early winter, with  
 235 a prominent trough in late summer. Spring peak  $Q$  coincided noticeably with a  
 236 separation in water temperature between SD and RS, while the summer trough  
 237 coincided with separation of RD and  $T_{\text{air}}$ . On average, November marked both  
 238 the autumn peak in  $Q$  and the point at which  $T_{\text{air}}$  fell below  $T_{\text{water}}$ .

239 There was also an apparent divergence in slope between RD and all snow-  
 240 influenced rivers, beginning in early spring and culminating in June. Between  
 241 June and July, RS and SD saw a large jump in temperature, which coincided  
 242 with the decline in snowmelt.

243



244



245

246 **Figure 3** (a-c) Relationships between watershed elevation and climatic effects  
 247 on  $T_{\text{water}}$ , obtained from full model fit. (d-e) Relationships between watershed  
 248 features and factor loadings on shared trends, from constrained model fit. Re-  
 249 gression lines indicate slopes significant at  $\alpha = 0.1$ . (f) Ordination of landscape  
 250 predictors by principal coordinates analysis. Length and direction of arrows are  
 251 proportional to loading of landscape predictors onto each principal axis of their  
 252 variation.

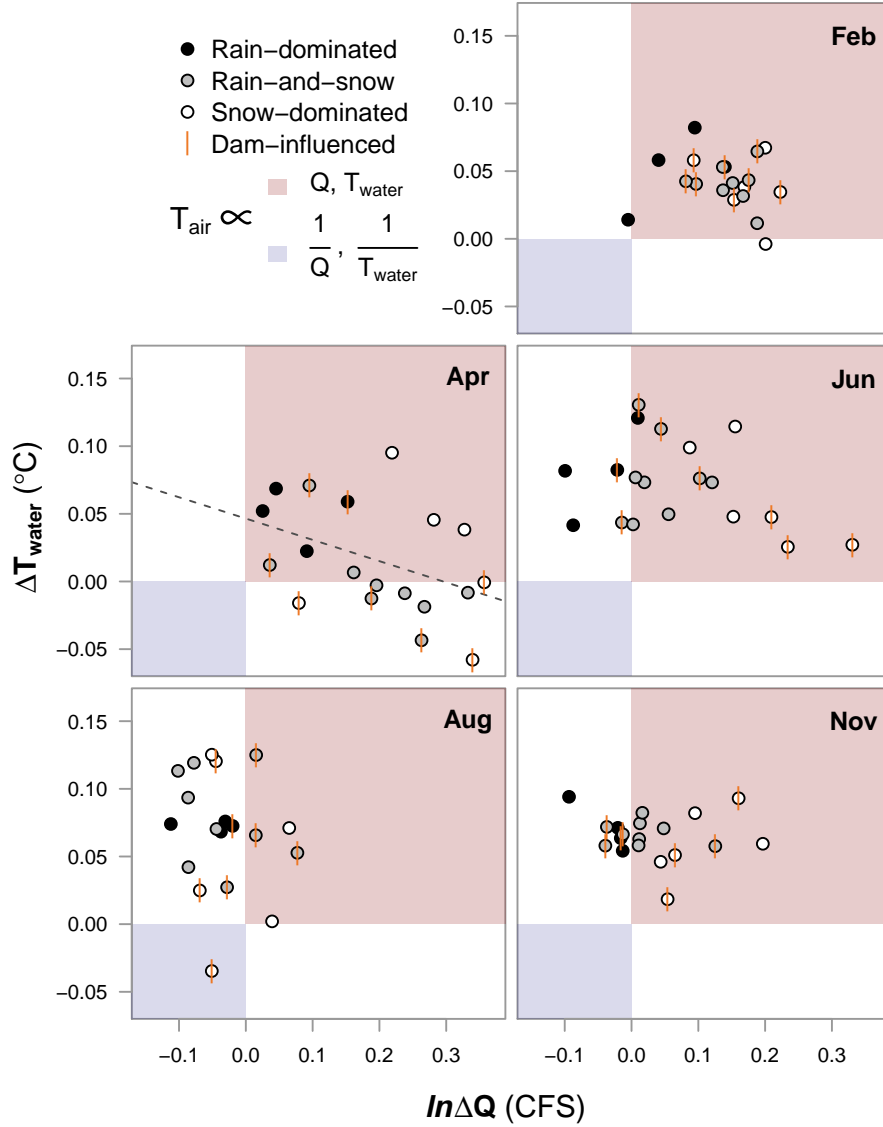
253

254 DFA results, aggregated across months and years for each site, revealed a  
 255 trend toward reduced  $T_{\text{air}} \rightarrow T_{\text{water}}$  coupling with increasing watershed el-  
 256 evation ( $p = 0.04$ ,  $\text{mult.}R^2 = 0.18$ ; Fig. 3a). On average, a  $1^\circ\text{C}$  change in  
 257  $T_{\text{air}}$  corresponded to a  $0.53 \pm 0.03^\circ\text{C}$  change in  $T_{\text{water}}$  at RD, a  $0.51 \pm 0.08^\circ\text{C}$   
 258 change at RS, and a  $0.45 \pm 0.17^\circ\text{C}$  change at SD sites. A similar trend was  
 259 observed with respect to  $\text{precip} \rightarrow T_{\text{water}}$  coupling ( $p = 0.03$ ,  $\text{mult.}R^2 = 0.21$ ;  
 260 Fig. 3b), where a monthly change in total precipitation of 1 cm corresponded

261 to a  $0.02 \pm 0.009^{\circ}\text{C}$  change in  $T_{\text{water}}$  for RD,  $-0.003 \pm 0.009^{\circ}\text{C}$  for RS, and  
 262  $0.004 \pm 0.02^{\circ}\text{C}$  for SD. There was no evidence of coupling overall between  
 263 snowmelt and  $T_{\text{water}}$  (Fig. 3c), but this predictor was included in the most  
 264 parsimonious DFA model selected via AIC and  $R^2$  (See Appendix A.). The  
 265 strongest examples of  $T_{\text{air}} \rightarrow T_{\text{water}}$  and  $\text{precip} \rightarrow T_{\text{water}}$  coupling were ob-  
 266 served in the Duckabush River, while the weakest examples are from the Elwha  
 267 River. Both rivers drain glaciers of the Olympic Mountain Range, and both are  
 268 SD. Among SD rivers, those influenced by dams appear to couple less strongly  
 269 with  $T_{\text{air}}$  and  $\text{precip}$ , but more so with snowmelt.

270 Factor loadings from a constrained, two-trend model each correlated with  
 271 one of the two dominant, principal axes of variation across landscape predictors,  
 272 determined by PCoA (Fig. 3f). The first principal axis was driven by mean  
 273 watershed slope, snow (% area  $> 1000$  m) and ice, soil permeability, and other  
 274 features that vary along elevational gradients, as well as mean elevation itself.  
 275 Watershed's scores along this axis correlated with loadings from one trend, with  
 276 marginal significance ( $p = 0.07$ ,  $\text{mult.}R^2 = 0.14$ ; Fig. 3d). The second principal  
 277 axis was driven by runoff, base flow, and upstream dams, and correlated with  
 278 the other trend's loadings ( $p < 0.01$ ,  $\text{mult.}R^2 = 0.35$ ; Fig. 3e). Combined,  
 279 the first two principal axes accounted for 79.4% of variation across landscape  
 280 predictors.

281



282

283 **Figure 4** Relationship between  $T_{\text{air}} \rightarrow T_{\text{water}}$  and  $T_{\text{air}} \rightarrow Q$ . Both axes are  
 284 expressed per  $1^{\circ}\text{C}$  change in  $T_{\text{air}}$ . The red quadrant designates proportionality  
 285 between all three variables, the blue inverse proportionality between each re-  
 286 sponse and  $T_{\text{air}}$ . Regression lines indicate slopes significant at  $\alpha = 0.05$ .

287

288 To examine possible sub-season interactions between  $T_{\text{air}}$ ,  $T_{\text{water}}$  and  $Q$ , we  
 289 performed an additional DFA with  $Q$  as the response. In both models,  $T_{\text{air}}$

was allowed to have unique monthly effects. These effects, taken together, can be conceptualized in relation to the four quadrants of the Cartesian coordinate system (increasing clockwise from upper right; Fig. 4).

In mid-winter (exemplified by February), all river classes primarily occupy the first quadrant, signifying  $T_{\text{air}} \propto T_{\text{water}}$  and  $T_{\text{air}} \propto Q$ , where  $\propto$  denotes proportionality. RD shows the weakest  $Q$  response. By spring, many RS and SD sites develop an inverse relationship between  $T_{\text{air}}$  and  $T_{\text{water}}$ , denoted  $T_{\text{air}} \propto \frac{1}{T_{\text{water}}}$ , while RD sites change little from their winter state. June and August see a procession of most sites into the near fourth quadrant, with SD trailing. This signifies  $T_{\text{air}} \propto \frac{1}{Q}$ , though  $T_{\text{air}} \propto T_{\text{water}}$ . One stark exception is again the Elwha river, which occupies quadrant three. By fall, RS and SD have begun progress back toward their winter states, led by SD. RD, meanwhile, remain essentially unmoved from summer.

Rivers influenced by dams do not appear to deviate appreciably from the rest in February, August, or November. However, SD rivers in April divide across the x-axis according to whether they are dammed. Those with dams exhibit  $T_{\text{air}} \propto \frac{1}{T_{\text{water}}}$ , while  $T_{\text{air}} \propto T_{\text{water}}$  for those without. Similarly, in June, dammed SD rivers display stronger coupling between  $T_{\text{air}}$  and  $Q$  than those without dams.

## Discussion

The effects of climate on  $T_{\text{water}}$ , inferred through dynamic factor analysis, suggest that nearly all rivers included in our dataset were influenced strongly by air temperature, precipitation, and/or snowmelt across 38 years of monthly data (Fig. 3a-c). At most monitoring sites,  $T_{\text{water}}$  closely tracked changes in  $T_{\text{air}}$ , on average responding to increases and decreases with proportional movements of up to 66% magnitude. However, some rivers only weakly track  $T_{\text{air}}$ , and patterns in the intensity of this coupling relate primarily to changing landscape features along an elevational gradient. Glaciation and yearly snow burden are prominent among these, and for reasons of ecological and hydrological implication, the primary focus of the following discussion, along with the interacting role of dams.

Before any analysis, a "buffering" effect (the inverse of coupling) of ice on river temperature can be seen in the yearly patterns of  $T_{\text{water}}$  relative to  $T_{\text{air}}$  (Fig. 2). The aggregate hydrograph peaks due to snowmelt from April to June, at the same time that the trajectories of RS and SD (snow-influenced rivers) start to drop off relative to RD. After snowmelt begins to subside, RS and SD recover with a noticeable jump. For rivers that receive glacial runoff (SD), this buffering effect appears to remain into the summer months, guarding them from temperature rise when RS rivers instead approach the temperature of RD (Fig. 4). In an extreme case, the Elwha River was actually cooler in August during those years in which air temperature was higher, probably due to increased runoff from Carrie and Eel glaciers. The buffering effect of ice on river temperature is therefore two-fold, acting first on all snowmelt-influenced

333 rivers through a cold-water pulse in spring, and then on a subset of those rivers  
 334 throughout summer and fall, by way of glacial runoff. For RD rivers, which  
 335 receive little to no input from ice, summer temperature is entirely dictated by  
 336 that of the surrounding air, and any rain falling through it.

337 Temperature buffering by snow and ice appears to be enhanced by the action  
 338 of artificial impoundments. Eight sites on five rivers included in this study are  
 339 (or were until 2014, in the case of the Elwha River) interrupted by dams or  
 340 embankments that release stored water from the bases of their reservoirs. At 33  
 341 m, even the shallowest of these reservoirs is deep enough to stratify in summer,  
 342 meaning released water would come primarily from the cold hypolimnion (?).  
 343 This certainly would have affected temperature readings for the Green, Elwha,  
 344 Cedar and upper Skagit River sites, whose mainstems are or were dammed up-  
 345 stream of the sample location. The impact of damming on temperature readings  
 346 at the Skokomish and the lower Skagit River sites should be lesser, as major,  
 347 unobstructed river forks intercede between sample location and dam. These  
 348 sites are RS and SD, respectively, and both fall almost exactly on the regression  
 349 line in Figure 4a. The upper Skagit site therefore occupies a middling space of  
 350  $T_{air} \rightarrow T_{water}$  coupling between "fully" obstructed and unobstructed SD sites.

351 As for the unobstructed SD sites, they appear to oppose the trend exempli-  
 352 fied overall. In particular, the Duckabush and Puyallup Rivers noticeably break  
 353 suit with the rest in terms of precip.  $\rightarrow T_{water}$  and  $T_{air} \rightarrow T_{water}$ , showing  
 354 stronger relationships even than many of the RD rivers (upper white circles in  
 355 Figs 3a, 3b, and 4-Apr.). Compared to the other rivers, these stand out in terms  
 356 of mean water table depth and base flow index (Appendix C)

357 all RD and RS rivers, as well as most SD, these two stand out in terms of  
 358 mean watershed slope and water table depth (not shown). Steeper slope may...  
 359 and coincide with smaller streams...

360 but dams aren't creating this effect on their own. they're augmenting it.  
 361 evaluate in context of RS

362 The effect of this (?) (?)

363 link to next paragraph... wtdep+ om-

364 Though higher-elevation watersheds will always produce colder water, inde-  
 365 pendent of the influence of ice and snow, it can be expected that RS and SD  
 366 rivers will grow more similar to RD as regional temperatures warm and glaciers  
 367 decline. That is to say, formerly reliably cold-water streams and associated  
 368 habitats may see increases in both summer and winter average temperatures,  
 369 as well as higher variability from year to year. The Elwha in particular may  
 370 slip from its current state of high resistance to seasonal climatic changes. We  
 371 tested for changes in mean and variance of  $T_{air} \rightarrow T_{water}$  and  $T_{air} \rightarrow Q$  coupling  
 372 between 1978 and 2015, but did not detect any regular patterns (Appendix B).

373 In addition to the three climate predictors, five shared trends were fit by the  
 374 most parsimonious DFA model. These represent additional drivers responsible  
 375 for structuring water temperature across some or all of the 24 sites included in  
 376 the analysis. Each monitoring sites' factor loading on a particular shared trend  
 377 indicates the degree to which the trend accounted for variance in  $T_{water}$  at  
 378 that site. While the precise identities of these drivers cannot be obtained with



379 certainty, they can be inferred through correlation with predictor variables.  
 380 In this way, we determined the most likely landscape drivers of  $T_{\text{water}}$  to be  
 381 perennial ice and snow cover, mean watershed slope, and groundwater influx.  
 382 In the case of slope, the likely mechanism of influence is increased turbulence and  
 383 mixing of water and air in steep, headwater streams, which allows convective  
 384 warming and cooling to occur more rapidly ?; Fig. 3g). As for groundwater,  
 385 greater influx (represented by baseflow index, or BFI; fig. 3f) corresponds to  
 386 greater *de*-coupling of climatic effects and river temperature, as groundwater  
 387 should be insulated relative to surface water. For the same reason, greater depth  
 388 of groundwater should be associated with better insulation and thus further  
 389 decoupling (Fig. 3d). The buffering effect of perennial ice and snow on SD  
 390 rivers has already been discussed, but the uniquely high factor loadings of RS  
 391 rivers in relation to the associated trend are worth noting (Fig. 3e). This trend  
 392 may account for variation in RS due to traits shared by RD and SD, or to a  
 393 "rain-on-snow" effect that may yield additional cold water in early spring. The  
 394 fifth trend did not correlate strongly with any of the landscape predictors in our  
 395 dataset. It may therefore represent additional, unknown drivers like marine or  
 396 microclimatic effects, or it may simply account for random noise.

397 The relationship between climate and river temperature is further influenced  
 398 by the interaction of Q, and the fates of rivers in the Puget Sound watershed can  
 399 be best understood by examining these factors in combination (Fig. 4). Whether  
 400 rain-, both-, or snow-dominated, all rivers took on RD characteristics in winter,  
 401 when the effects of ice lay latent. As a result, warmer Februaries on average  
 402 yielded warmer rivers and higher flow (less precipitation bound in ice). The  
 403 critical differences between river classes played out in spring and summer, and  
 404 it's during these months that future perturbations due to changing climate may  
 405 be felt most acutely. For example, warmer Aprils on average produced colder  
 406 water at 9 out of 15 RS and SD sites. Though we determined Q, groundwater,  
 407 and slope to be likely components of this relationship, only melting ice could  
 408 be credited with actually reversing it. Projected reductions in snowpack for the  
 409 Pacific Northwest can therefore be expected to fundamentally alter the responses  
 410 of currently snow-influenced rivers to yearly variation in spring temperature.  
 411 In the longer term, changes can be expected for rivers that now receive the  
 412 temperature-buffering effect of glacial runoff. Glaciers continue to decline across  
 413 North America, with glacial ice across Western Canada projected to decline by  
 414 70% from 2005 to 2100 (?).

## 415 Conclusion

416 Temperature regimes across the rivers of the Puget Sound watershed are struc-  
 417 tured by a combination of climatic drivers at the regional scale, and geophysical  
 418 drivers at watershed scales. In the absence of snow and ice, river temperature is  
 419 closely coupled to that of the surrounding air, while contributions of snowmelt  
 420 and glacial runoff can dampen or even reverse this coupling in spring and sum-  
 421 mer. In some cases, icemelt-influenced rivers exhibit stronger positive responses

422 to climate patterns than their rain-driven counterparts. Our results suggest ele-  
423 vational variations in groundwater influx, total  $Q$ , and watershed slope account  
424 for these patterns. However, while these factors may influence the degree of cou-  
425 pling between climatic drivers and water temperature, only snow and ice can  
426 reverse it. Since 1978, such reversals have been widespread, particularly during  
427 spring melt. Though we did not detect changes in this effect across histori-  
428 cal observations, future reductions in snowpack and glacial mass are projected.  
429 Consequently, many rivers that now undergo the mildest seasonal temperature  
430 changes may be impacted most strongly.

## Appendix A

### Temperature DFA output and diagnostics

Model selection included four climate covariates (air temperature, precipitation, snowmelt, and hydrological drought), between 1 and 15 shared trends, four within-and-among-site error structures (see methods), and two models of unknown seasonal variation (fixed monthly factors and Fourier series). The most parsimonious model of river temperature was selected using the Akaike Information Criterion (AIC), and included air temperature, precipitation, and snowmelt as covariates. This model also included five shared trends and an independent and unequally distributed error structure among streams (i.e. diagonal and unequal variance-covariance matrix).

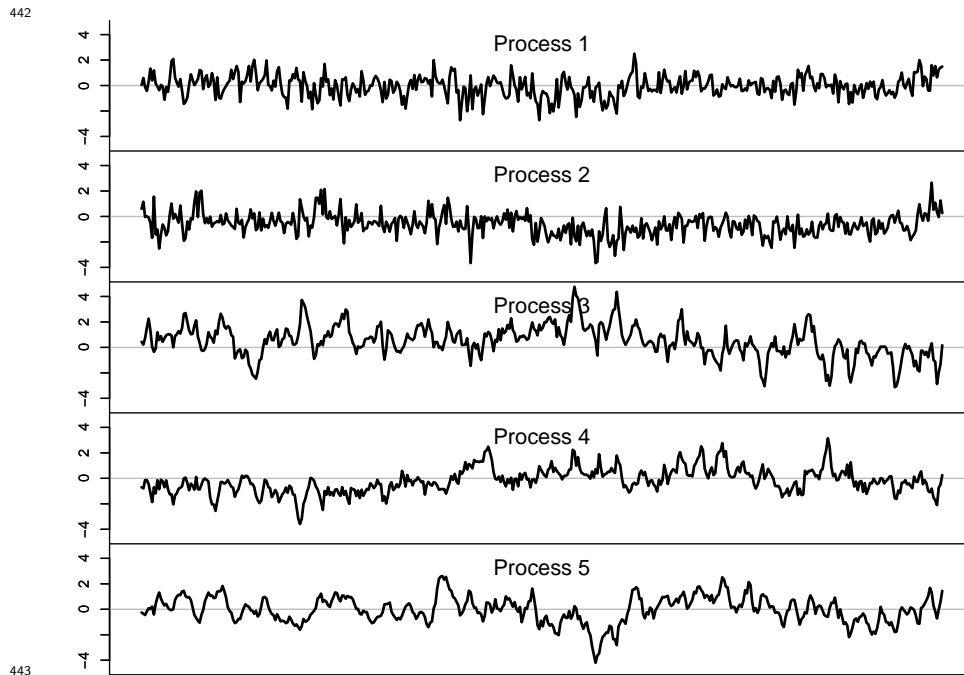
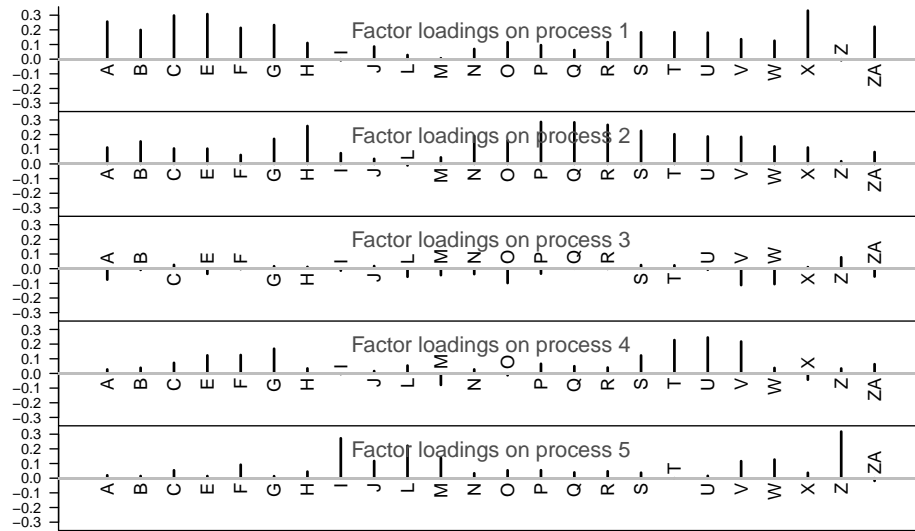
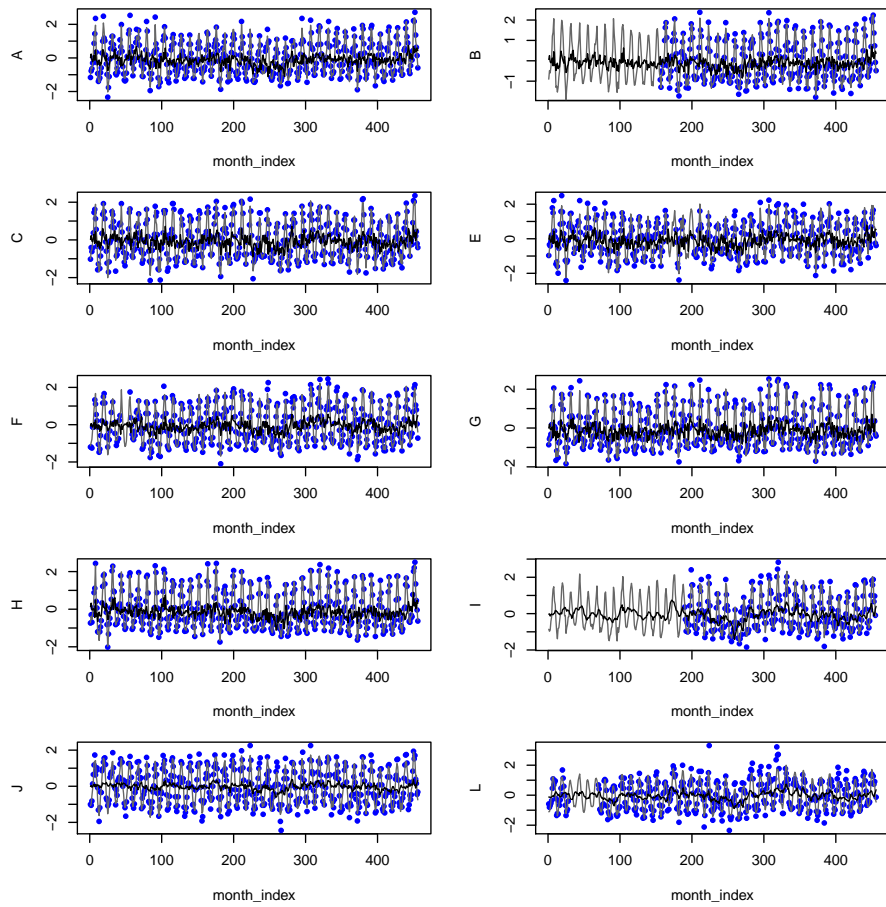


Figure A1 Shared trends.



**Figure A2** Factor loadings on shared trends.



**Figure A3** Model fits (gray line = overall; black line = trends-only).

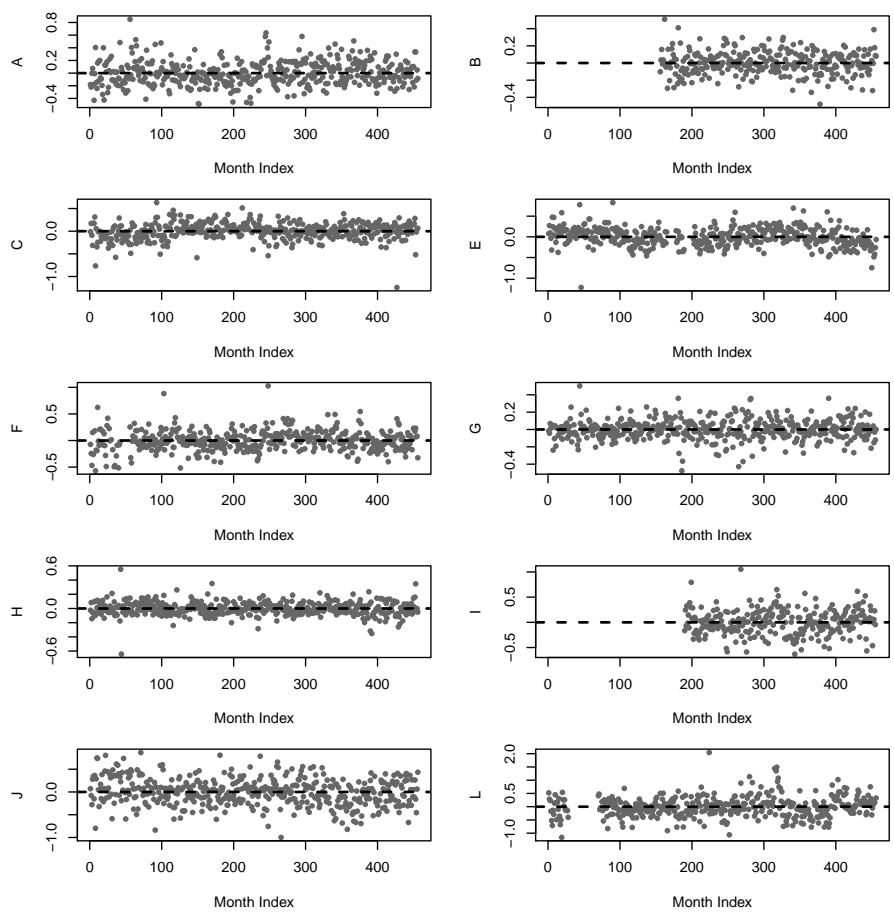
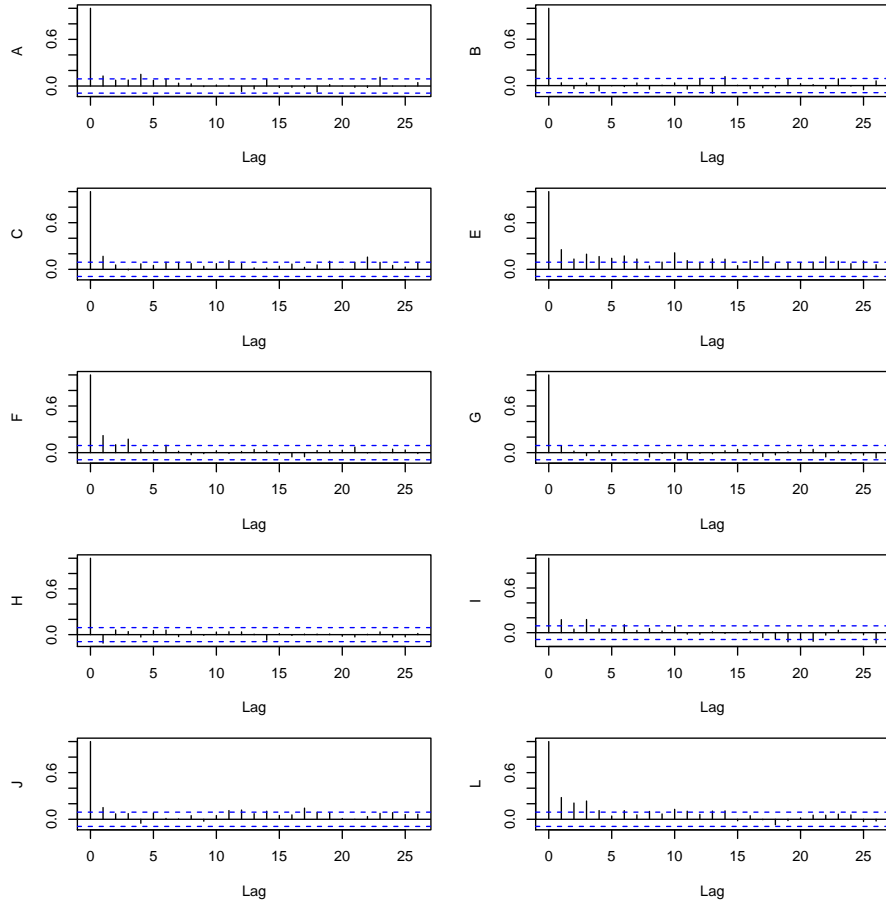


Figure A4 Residuals.



**Figure A5** Autocovariance function (ACF).

Output from the discharge model looks very similar to this, and is omitted here for the sake of retaining a reasonable page count.

## Appendix B

### Testing for change in coupling over time

We used an additional DFA model to test for changes in  $T_{air} \rightarrow T_{water}$  coupling over time, by dividing the 1978-2015 time series into 5 intervals and comparing central tendency and variance of effect sizes for each interval. Figures B1-B3 show mean effect size for each stream.

To approximate estimates of variability over time, we performed the same analysis within a Bayesian framework, and obtained uncertainty estimates from the credible intervals of the effect size posteriors. This approach yielded no trends in variation over time, and is not visualized here (This will be included in the final version of this paper).

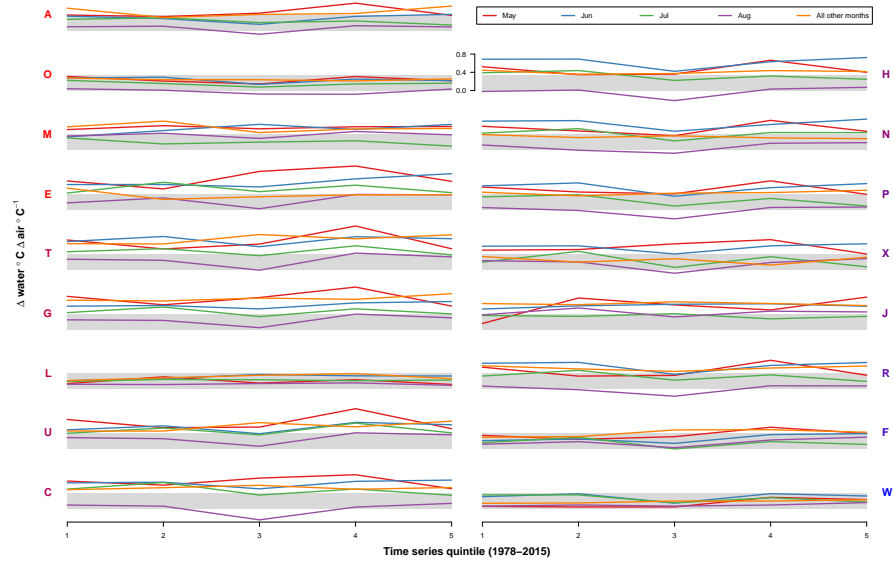


**Figure B1** Mean  $T_{air} \rightarrow T_{water}$  coupling over time. Each plot corresponds to an individual site. Y-label colors represent mean watershed elevation (bluer=higher).



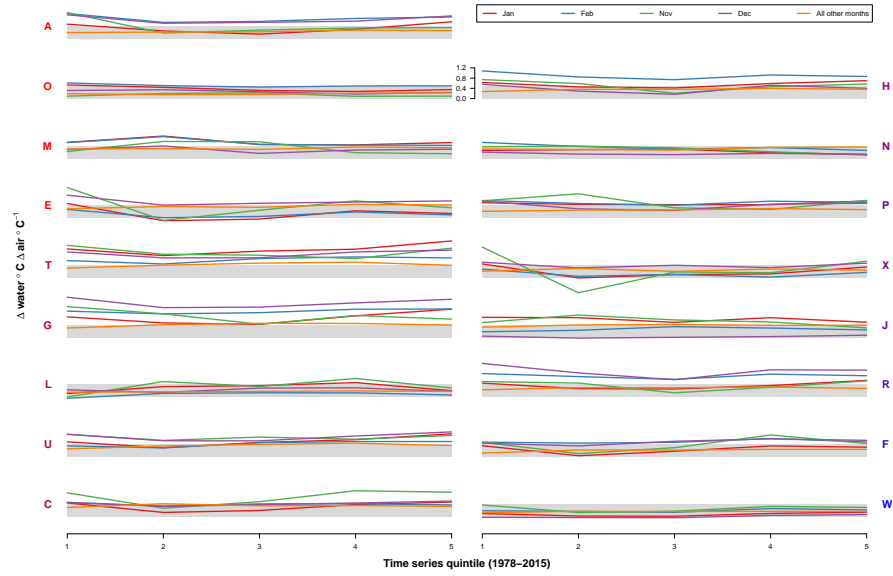


**Figure B2** Mean  $T_{air} \rightarrow T_{water}$  coupling over time. Each plot corresponds to an individual site. Y-label colors represent mean watershed elevation (bluer=higher).

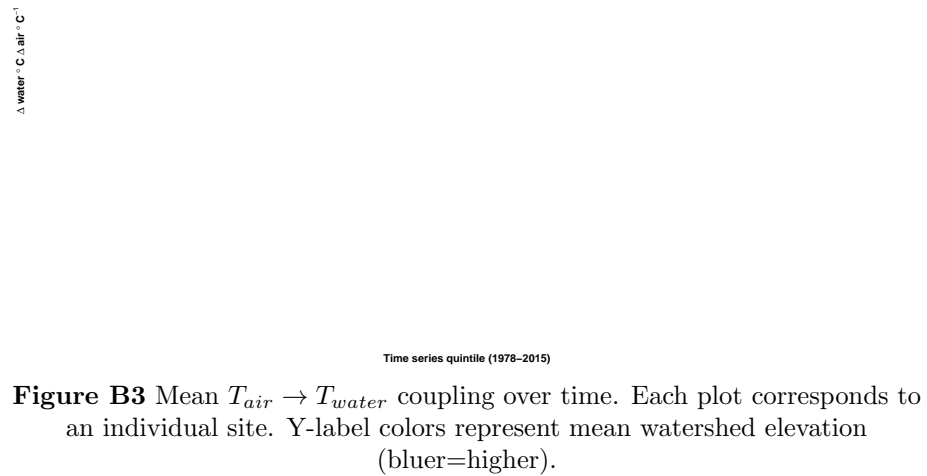


**Figure B3** Mean  $T_{air} \rightarrow T_{water}$  coupling over time. Each plot corresponds to an individual site. Y-label colors represent mean watershed elevation (bluer=higher).

485 **Appendix C**

486 **Table C1.**

Site code	DoE ID	Description	Lat.	Long.	Site elev.	Elev.	Area	Area $\dot{z}$ 1000 m	Slope	Dammed
A	08C070	Cedar R @ Logan St/Renton	47.5	-122.2	4.6	611.3	457.1	0.3	18.1	yes
B	09A080	Green R @ Tukwila	47.5	-122.2	1.2	546.2	1115.7	0.6	23.5	yes
C	01A050	Nooksack R @ Brennan	48.8	-122.6	3	674.5	2046.2	0	5	no
E	03B050	Samish R nr Burlington	48.5	-122.3	11.6	268	225.3	0.2	16.7	no
F	03A060	Skagit R nr Mount Vernon	48.4	-122.3	4.3	1128.3	8035.1	0.2	15.4	partial
G	05A070	Stillaguamish R nr Silvana	48.2	-122.2	10.7	604.1	1456.7	0	6.8	no
H	07A090	Snohomish R @ Snohomish	47.9	-122.1	2.4	688.4	4449.9	0.5	19.2	no
I	16C090	Duckabush R nr Brimmon	47.7	-123	91.4	1047.5	178.6	0.2	13.5	no
J	10A070	Puyallup R @ Meridian	47.2	-122.3	9.1	921	2439.4	0.2	14.1	no
L	16A070	Skokomish R nr Potlatch	47.3	-123.2	18.3	608.8	591.7	0.2	17.1	partial
M	13A060	Deschutes R @ E St Bridge	47	-122.9	28.3	288.2	408.5	0.3	15.7	no
N	09A190	Green R @ Kanaskat	47.3	-121.9	236.2	822.2	659.1	0	5.3	yes
O	08C110	Cedar R nr Landsburg	47.4	-121.9	187.8	808.3	310.3	0.8	25.7	yes
P	07D130	Snoqualmie R @ Snoqualmie	47.5	-121.8	121.9	897.8	946.6	0	11.9	no
Q	07D050	Snoqualmie R @ Monroe	47.8	-122	4.6	638.1	1779.7	0.2	22.8	no
R	07C070	Skykomish R @ Monroe	47.9	-122	13.1	904.6	1986.9	0.3	14.5	no
S	05A110	SF Stillaguamish R nr Granite Falls	48.1	-122	88.4	768.7	308.1	0	8.1	no
T	05A090	SF Stillaguamish R @ Arlington	48.2	-122.1	16.8	625.2	657	0.4	15.7	no
U	05B070	NF Stillaguamish R @ Cicero	48.3	-122	33.5	665.5	667.4	0.4	18.3	no
V	05B110	NF Stillaguamish R nr Darrington	48.3	-121.7	132.6	714.2	222.5	0.3	15.6	no
W	04A100	Skagit R @ Marblemount	48.5	-121.4	109.7	1349.2	3601.1	0.4	14.6	yes
X	01A120	Nooksack R @ No Cedarville	48.8	-122.3	42.7	868.2	1542.7	0.2	9.9	no
Z	18B070	Elwha @ Port Angeles	48.1	-123.6	67.1	1088.6	757.1	0.6	27.5	yes
ZA	08B070	Sammamish R @ Bothell	47.8	-122.2	4.6	147.2	559.8	0.4	19.2	no

Site code	Perenn. ice	Runoff	Bedrock dep.	Water tbl. dep.	Soil perm.	Aspect	BFI	Rip. pop. dens.	Imp. surf.	Urb.	Road dens.
A	0.3	1238.8	143	135.1	14.2	290.6	61.3	81.6	2.9	5.5	3.4
B	2.2	1169.4	140.8	134.6	12.3	295.6	61.1	148.8	4.3	8.2	3.9
C	0	1714.2	139.3	127.2	9	269.1	58.4	26.9	1.2	2.2	1.4
E	0.2	1546	143.2	118.4	12	252.7	52.8	29.2	2.4	5.3	1.8
F	0.6	1998.6	133.5	145.3	7.5	260.8	61.3	5.6	0.6	1.2	0.6
G	0	2563.9	139.8	126.9	7.4	261.5	52	19.6	0.9	1.6	1.3
H	0.3	2255.7	137.2	135	10.9	277.8	57.2	38	1.7	3.5	1.9
I	0.1	1993.8	95.7	172.8	4.7	87.4	54.3	1	0.1	0	0.2
J	0.1	1204.2	145.8	144.4	12.2	295.1	61.5	48.2	2.3	4.5	1.7
L	0.1	1900	112.6	143	7.3	139.2	52.3	2.7	0.5	0.3	1.4
M	0.2	1261.1	139.8	157	17.1	317.2	59.4	70.4	2.1	3.5	2.9
N	0	1165	135.5	152.4	7.7	284.9	59.4	5	0.8	0.9	3.1
O	2.5	1239.9	141.1	139.2	10.4	271.3	59	4.3	0.7	0.5	2.6
P	0	2087.7	135.8	153.4	16.5	243	58.3	18.3	1.4	2.5	2
Q	4	2097.9	139.4	136.8	13.8	270.5	58.6	33.1	1.6	3.1	2.6
R	1.8	2605.6	133.1	143.8	9.3	277.5	56.4	11.1	1	2.1	1.1
S	0	2545	134.5	137.1	6.8	276	54.9	9.4	0.7	1.1	1
T	0	2557.2	137.6	129.5	6.9	280.1	52	23.4	1.1	1.9	1.4
U	0.1	2568.8	140.5	127.9	7.2	272.5	53.1	5.2	0.6	1	1
V	0.1	2562.5	138.2	134.1	6.4	254.4	57.4	3.7	0.5	0.7	1.1
W	3	1806.4	132.1	150.4	6.5	253.8	65.3	0.3	0.5	1.1	0.2
X	0	1715.1	136.6	137.1	7.2	257.9	58.7	5.4	0.6	0.8	1.2
Z	4.4	1599.4	118.3	175	7	323.4	60.4	1	0.1	0	0.2
ZA	2.3	1264.4	143.2	124.1	20.6	339.4	64.2	529.7	14.6	29	6.6